

Global optimization of dielectric metasurfaces using a physics-driven neural network

Jiaqi Jiang and Jonathan A. Fan*

Department of Electrical Engineering, Stanford University, Stanford, CA, USA

E-mail: jonfan@stanford.edu

Abstract

We present a global optimizer, based on a generative neural network, which can output highly efficient topology-optimized metasurfaces operating across a range of parameters. A key feature of the network is that it initially generates a distribution of devices that broadly samples the design space, and then shifts and refines this distribution towards favorable design space regions over the course of optimization. Training is performed by calculating the forward and adjoint electromagnetic simulations of outputted devices and using the subsequent efficiency gradients for backpropagation. With metagratings operating across a range of wavelengths and angles as a model system, we show that devices produced from the trained generative network have efficiencies comparable to or better than the best devices produced by adjoint-based topology optimization, while requiring less computational cost. Our reframing of adjoint-based optimization to the training of a generative neural network applies generally to physical systems that can utilize gradients to improve performance.

Keywords: Global optimization, generative neural networks, machine learning, adjoint variable method, metasurfaces, metagrating

Introduction

Metasurfaces are subwavelength-structured artificial media that can shape and localize electromagnetic waves in unique ways.¹⁻³ These technologies are useful in imaging,⁴⁻⁶ sensing,⁷ and optical information processing applications,⁸ amongst others, and can operate at wavelengths spanning the ultraviolet to radio frequencies.⁹⁻¹¹ A central research thrust in the field has been the identification of effective and computationally efficient ways to design high performance metasurfaces, given a desired electromagnetic response.¹² In this aim, inverse design based on optimization has shown great promise. These methods range from heuristic swarm¹³ and genetic algorithms^{14,15} to adjoint-based topology optimization,^{16,17} and they have led to metagratings,^{18,19} metasurfaces,²⁰⁻²² and other nanophotonic devices²³⁻²⁵ with exceptional performance. However, they are computationally costly, making it difficult and even intractable to scale these methods to large ensembles of devices or large area devices.

To address this computational roadblock, concepts in machine learning have been investigated as a means to generate device layouts without requiring computationally-costly electromagnetic solvers.²⁶⁻²⁸ In current manifestations of machine learning-enabled photonics design, a training set of devices and their associated optical properties is first produced. These data are then used to train a neural network, which "learns" the relationship between device geometry and optical response. A properly trained network can then produce new device designs beyond the training dataset, at low computational cost. To date, a range of machine learning concepts, including deep neural networks with fully connected networks, convolutional networks, and generative adversarial networks (GANs), have been proposed.²⁹⁻³¹

These initial demonstrations show that neural networks have the potential to learn the relationship between structural geometry and optical response, but they also highlight key challenges to the approach.^{26,29} One challenge is that the computational cost of creating the training dataset itself can be immense. Networks for structures described by even a few geometric parameters require tens to hundreds of thousands of devices for training. GAN-based

design strategies have the potential to work with relatively less training data, but these data are pre-optimized and are computationally costly to produce.^{30,31} Another challenge is that many nanophotonic devices have complex curvilinear geometries and reside in a high dimensional design space, making it difficult for even the best networks to learn the nuanced relationship between device geometry and response. New concepts that extend beyond standard machine learning approaches are required for neural networks to be practically useful in the electromagnetics design process.

In this Letter, we introduce a new concept in electromagnetic device design by incorporating adjoint variable calculations directly into generative neural networks. Termed global topology optimization networks (GLOnets), our approach is capable of generating high performance topology-optimized devices spanning a range of operating parameters with modest computational cost. GLOnets work by initially evaluating a distribution of devices spanning the design space and then continuously optimizing this device distribution until it converges to a cluster of high efficiency devices. Physics-based gradients are utilized to ensure that network training is directly tied with enhancing device efficiency. We note that while our network performs a global search within the design space, it does not ensure that the final generated devices are globally optimal. In general, it is not possible to solve for global optima in non-convex optimization problems, including our problem. As a model system, we use GLOnets to design an ensemble of silicon metagratings that operate across a range of wavelengths and deflection angles.

Methods

Our metagratings consist of silicon nanoridges and deflect normally-incident light to the +1 diffraction order (Figure 1a). The thickness of the gratings is fixed to be 325 nm and the incident light is TM-polarized. For each device, the metagrating period is subdivided into $N = 256$ segments, each with a refractive index value between silicon and air. These refractive

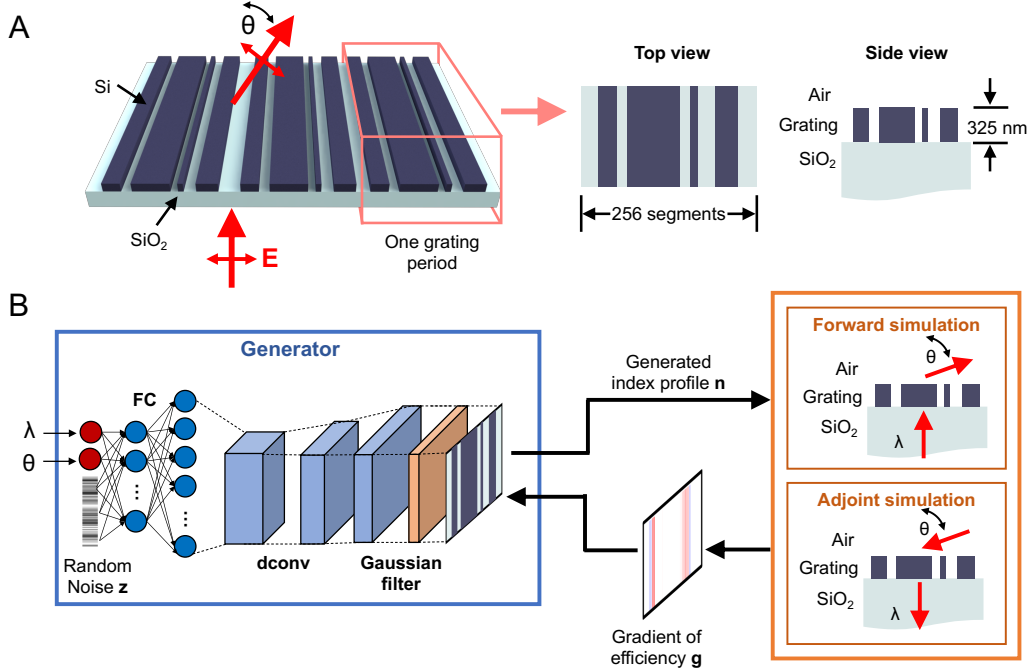


Figure 1: **Global optimization based on a generative neural network.** (A) Schematic of a silicon metagrating that deflects normally incident TM-polarized light to the outgoing angle θ . The metagrating consists of 325nm-thick Si ridges in air on a SiO₂ substrate. In the generative neural network, the device is specified by a 1×256 vector, \mathbf{n} , which represents the refractive index profile of one period of the grating. (B) Schematic of GLOnet for metagrating generation. The generator is built on fully connected layers (FC), deconvolution layers (dconv), and Gaussian filters. The input is the device wavelength λ , deflection angle θ , and an 8-dimensional noise vector \mathbf{z} , and the output is the device vector \mathbf{n} . During each iteration of training, a batch of devices is generated and efficiency gradients \mathbf{g} are calculated for each device using forward and adjoint electromagnetic simulations. These gradients are backpropagated through the network to update the weights of the neurons.

index values are the design variable in our problem and are specified as \mathbf{n} (a $1 \times N$ vector). Index values in the vector are normalized to a range of -1 , which represents air, and $+1$, which represents silicon. The optimization objective is to maximize the deflection efficiency of the metagrating given an operating wavelength ranging from 600 nm to 1300 nm and an outgoing angle ranging from 35 degrees to 85 degrees.

A schematic of our GLOnet is presented in Figure 1b. The input is the operating wavelength λ , the desired outgoing angle θ , and an 8-dimensional noise vector \mathbf{z} , which is a uniformly distributed random variable. The output is the refractive index profile of the device,

n. The weights of the neurons are parameterized as **w**. Initially, the weights in the network are randomly assigned and different **z** map onto different device instances: $\mathbf{n} = G_{\mathbf{w}}(\mathbf{z}; \lambda, \theta)$. In this initial network state, the ensemble of noise vectors $\{\mathbf{z}\}$ maps onto an ensemble of device instances $\{\mathbf{n}\}$ that span the device design space.

During network training, the goal is to iteratively optimize **w** to maximize the objective function $L^* = \overline{\text{Eff}}$, where $\overline{\text{Eff}}$ is the average efficiency of the ensemble $\{\mathbf{n}\}$. To improve **w** each iteration, a batch of M devices is initially generated by sampling **z** from the noise vector distribution, λ from the target wavelength range, and θ from the target outgoing angle range. The gradients of efficiency with respect to **n**, which specify how the device indices can be modified to improve the objective function, are then calculated for each device. For the i^{th} segment of the m^{th} device, which has the refractive index $n_i^{(m)}$, this gradient normalized to M is defined as $\frac{1}{M}g_i^{(m)} = \frac{\partial L^*}{\partial n_i^{(m)}}$. To express the objective function in an explicit form for backpropagation, we redefine the objective function to be:

$$L = \frac{1}{M} \sum_{m=1}^M \sum_{i=1}^N n_i^{(m)} \cdot g_i^{(m)} \quad (1)$$

The gradient of this objective function with respect to the index, at the i^{th} output neuron for the m^{th} device, is $\frac{\partial L}{\partial n_i^{(m)}} = \frac{1}{M}g_i^{(m)} = \frac{\partial L^*}{\partial n_i^{(m)}}$, matching the desired efficiency gradient. To calculate the gradients applied to **w** each iteration, we backpropagate the efficiency gradients for each of the M devices and average the subsequent gradients on **w**.

The efficiency gradients $g_i^{(m)}$ are calculated using the adjoint variables method, which is used in adjoint-based topology optimization. These gradients are calculated from electric and magnetic field values taken from forward and adjoint electromagnetic simulations.¹⁹ We can therefore view our use of a neural network, in which the non-linear mapping between $(\mathbf{z}, \lambda, \theta)$ and device layout is iteratively improved using physics-driven gradients, as a reframing of the adjoint-based optimization process. Unlike other manifestations of machine learning-enabled photonics design, our approach does not use or require a training set of known

devices but instead learns the physical relationship between device geometry and response directly through electromagnetic simulations.

To ensure that the generated devices are binary, we add $|n_i^{(m)}|(2 - |n_i^{(m)}|)$ as regularization terms to the objective function. These terms reach a maximum when $|n_i^{(m)}| = 1$ and the device segments consist of either silicon or air. The gradients of these terms with respect to $|n_i^{(m)}|$ decrease linearly as $|n_i^{(m)}|$ approaches 0, and it becomes 0 when $|n_i^{(m)}|$ is zero. This binarization condition serves as a design constraint that limits metagrating efficiency, as the efficiency enhancement term (Equation 2) favors grayscale patterns. To balance binarization with efficiency enhancement in the objective function, we include the tunable hyperparameter β . Our final expression for the objective function is now:

$$L = \frac{1}{M} \sum_{m=1}^M \sum_{i=1}^N [n_i^{(m)} \cdot g_i^{(m)} + \beta \cdot |n_i^{(m)}|(2 - |n_i^{(m)}|)] \quad (2)$$

While GLONet uses adjoint-based gradients to optimize metagrating generation, it is qualitatively different from adjoint-based topology optimization. To conceptualize these differences, we discuss each optimization strategy in more detail. Adjoint-based topology optimization, as applied to a single device, is a local optimizer. The algorithm takes an initial dielectric distribution and enhances its efficiency by adjusting its refractive indices at each segment using gradient ascent (Figure 2a). This method is performed iteratively until the device reaches a local maximum in the design space. The performance of the final device strongly depends on the choice of initial dielectric distribution.³² More of the design space can be explored with this approach by performing topology optimization on many devices, each with different initial dielectric distributions. Devices that happen to have initial dielectric distributions in favorable design space regions will become high performing.

Local optimizers are an effective tool to designing a wide range of photonic devices. However, their usage is accompanied by a number of caveats. First, they require significant computational resources. Hundreds of electromagnetic simulations are required to topology

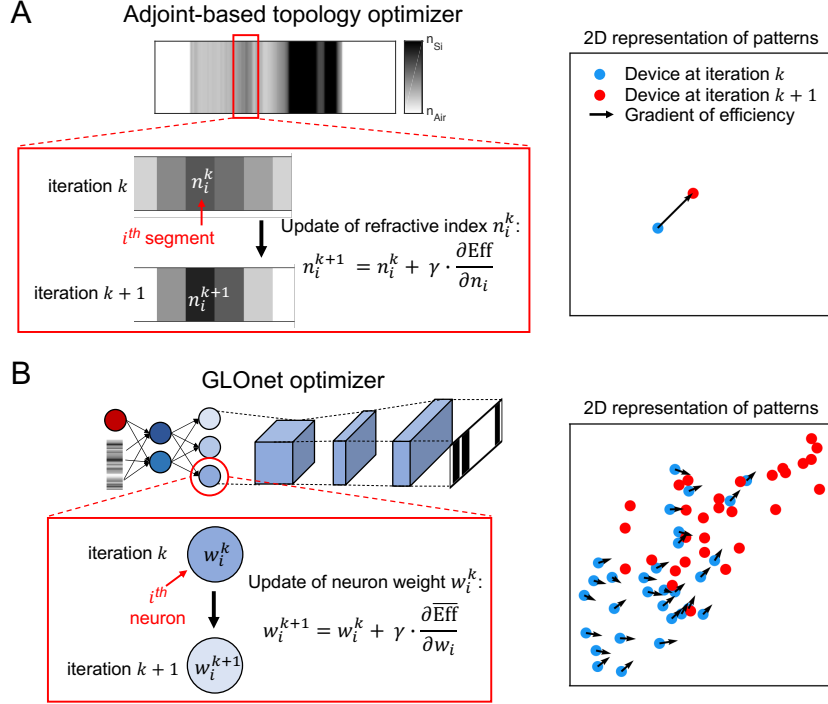


Figure 2: **Comparison between adjoint-based topology optimization and GLOnet optimization.** (A) Adjoint-based topology optimization uses efficiency gradients from an individual device to improve its performance within the local design space. A visualization of the device in a 2D representation of the design space illustrates that from iteration k to $k + 1$, the device moves incrementally to a nearby local maxima, indicated by its local gradient. (B) GLOnet uses a neural network to map random noise to a distribution of devices. Gradients of efficiency, averaged over a batch of devices, are backpropagated to update the weights of the neurons and deconvolution kernels, which improves the average efficiency of the device distribution. A visualization of the device distribution illustrates that from iteration k to $k + 1$, the efficiency gradients from individual devices (black arrows) are used to collectively bias the device distribution towards high efficiency regions of the design space.

optimize a single device, and for many devices, this number of simulations can scale to very large numbers. Second, the sampling of the design space is limited to the number of devices being optimized. For complex devices described by a very high dimensional design space, this sampling may be insufficient. Third, the devices locally optimize independently of one another, such that gradient information from one device does not impact other devices.

GLOnet is qualitatively different in that it optimizes an entire distribution of device instances, as represented by the noise vector. The starting point of each GLOnet iteration

is similar to adjoint optimization and involves the calculation of efficiency gradients for individual devices using the adjoint method. However, the difference arises when these gradients are backpropagated into the network. When considering the backpropagation of the efficiency gradient from even a single device, all the weights in the network get updated, thereby modifying the mapping of the entire distribution of device instances to device layouts (Figure 2b). This points to the presence of crosstalk, in which the gradients from one device influence other device instances. Crosstalk can be useful when devices in promising parts of the design space statistically exhibit particularly large gradients and more strongly bias the overall distribution of device instances to these regions. Devices stuck in sub-optimal local maxima of the design space can be biased away from these regions. Regulation of the amount of crosstalk between devices, which is important to stabilizing the optimization method, is achieved from the non-linearity intrinsic to the neural network itself.

Our GLOnet approach presents other additional advantages. One is that GLOnet is effective at broadly surveying the design space, enhancing the probability that optimal regions of the design space are sampled and exploited. Such global surveying is made possible in part because the input noise represents a continuum of device instances spanning the high dimensional design space, and in part because different subsets of devices are sampled each iteration, leading to the cumulative sampling of different regions of the design space early in the training process.

Another advantage is that GLOnet enables the simultaneous optimization of devices designed across a continuum of operating parameters in a single network training session. For our metagratings, these parameters include the outgoing angle and wavelength, each spanning a broad range of values. This co-design leads to a substantial reduction in computation time per device and is made possible because these devices operate with related physics and strongly benefit from crosstalk from the network training process.

Results and discussion

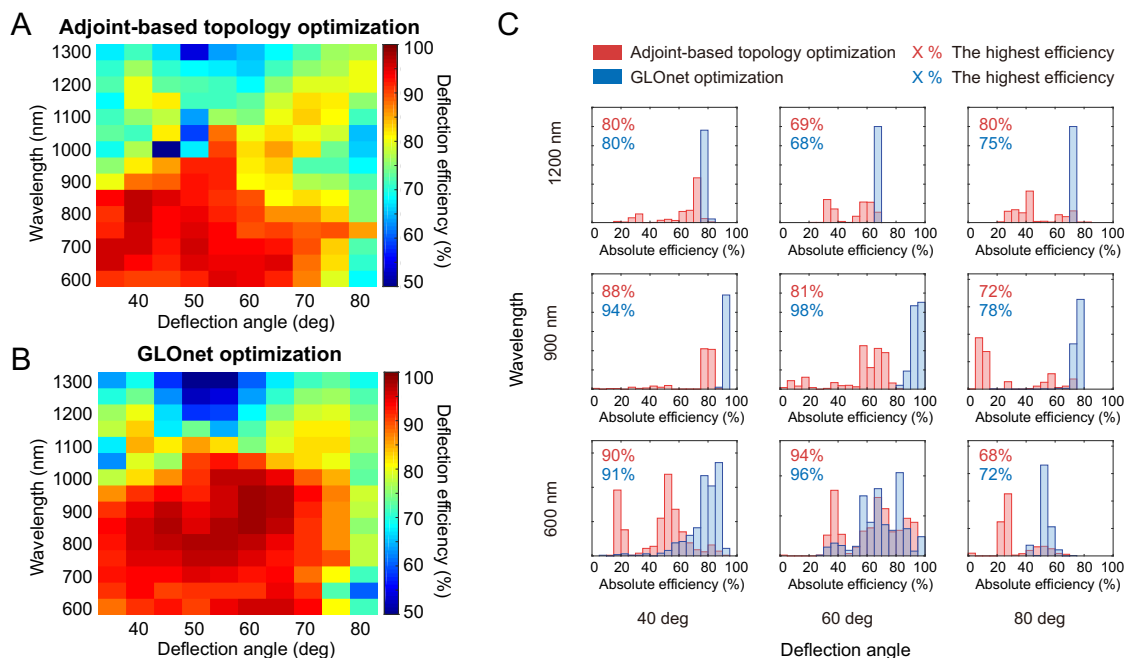


Figure 3: **Performance comparison of adjoint-based topology optimization and GLONet optimization.** (A) Plot of metagrating efficiency for devices operating with different wavelength and angle values, designed using adjoint-based topology optimization. For each wavelength and angle combination, 500 individual optimizations are performed and the highest efficiency device is used for the plot. (B) Plot of metagrating efficiency for devices designed using GLONet. For each wavelength and angle combination, 500 devices are generated and the highest efficiency device is used for the plot. (C) Efficiency histograms of devices designed using adjoint-based topology optimization (red) and GLONet optimization (blue). The highest device efficiencies in each histogram are also displayed. For most wavelength and angle values, the efficiency distributions from GLONet are narrower and have higher maximum values compared to those from adjoint-based topology optimization.

To benchmark devices designed from GLONet, we first perform adjoint-based topology optimization on metagratings operating across our desired range of wavelengths and angles. Details pertaining to this calculation can be found elsewhere.^{31,32} These devices operate across a wavelength range between 600 nm and 1300 nm, in increments of 50 nm, and across a deflection angle range between 35 degrees and 85 degrees, in increments of 5 degrees. For each wavelength and angle pair, we optimize 500 devices, each with random grayscale

patterns serving as initial dielectric distributions. A total of 200 iterations is performed for each optimization, and the deflection efficiencies of the optimized devices are calculated using a rigorous coupled-wave analysis (RCWA) solver.³³ The efficiencies of the best device for each wavelength and angle pair are plotted in Figure 3a.

For the same wavelength and angle pairs, 500 devices are generated from GLOnet by sampling \mathbf{z} 500 times. The efficiencies of the best devices are plotted in Figure 3b. Details pertaining to the architecture and training parameters are in the Supplementary Section. These efficiency values indicate that the best devices from GLOnet compare well with or are better than the best devices from adjoint-based optimization. Statistically, 57% of devices from GLOnet have efficiencies higher than those from adjoint-based optimization, and 87% of devices from GLOnet have efficiencies higher than or within 5% those from adjoint-based optimization. While GLOnet performs well for most wavelength and angle values, it does not optimally perform in certain regimes. We hypothesize that these nonidealities can be improved with further refinement of the network architecture and training process, and this will be the topic of future study.

The efficiency histograms from adjoint-based topology optimization and GLOnet, for select wavelength and angle pairs, are displayed in Figure 3c. A more complete set of histograms is shown in Figure S1. The histograms show that adjoint-based topology optimization generates devices with highly variable efficiencies. This indicates that the initial dielectric distributions of these devices broadly span the design space, and with each device being locally optimized, the result is a set of devices with a wide range of layouts and efficiencies. The GLOnet-generated devices, on the other hand, tend to have more devices clustered at the high efficiency end of the distribution. An examination of the layouts of these devices indicate that many have very similar geometries (Figure S2). This trend is consistent with the objective of GLOnet, which is to optimize the average efficiency of the distribution of generated devices.

To help visualize the process of device optimization with GLOnet, we show how the dis-

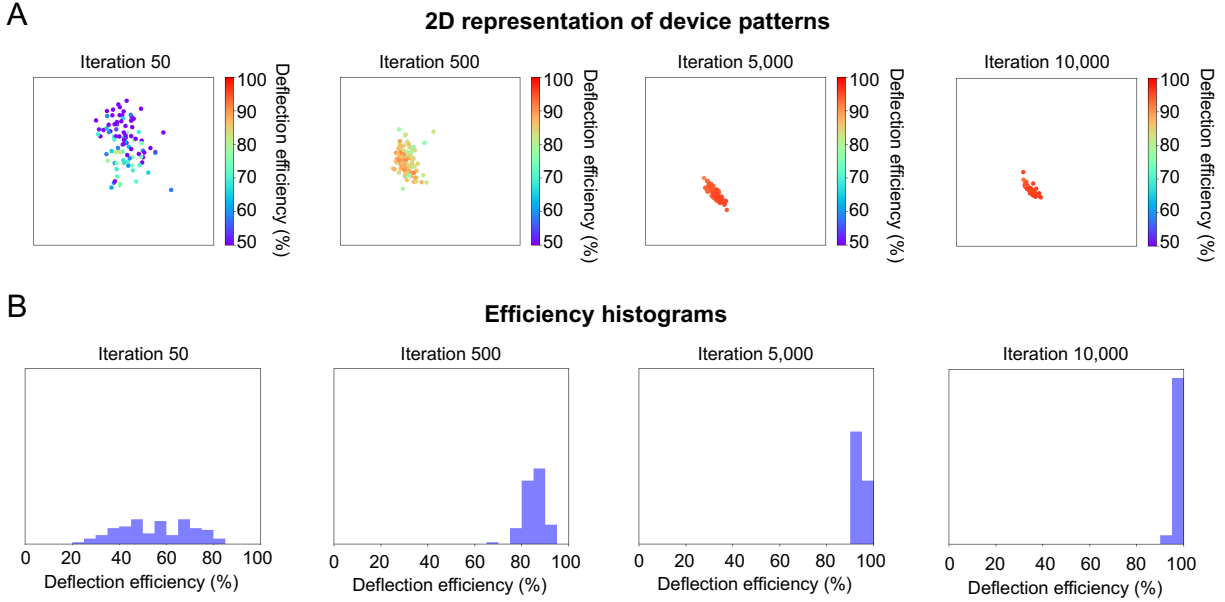


Figure 4: **Evolution of device patterns and efficiency histograms as a function of GLOnet training.** (A) Visualization of 100 device patterns generated by GLOnet at different iteration numbers, depicted in a 2D representation of the design space. All devices are designed to operate at a wavelength of 900 nm and an angle of 60 degrees. The distribution of generated devices is initially spread out in the design space at the early stages of training and converges to a high efficiency cluster by the 10,000 iteration mark. (B) Efficiency histogram of generated devices at different iteration numbers. The efficiency histogram is initially broad and converges to a sharp distribution of high efficiency devices by the 10,000 iteration mark.

tribution of devices in the design space, together with its corresponding efficiency histogram, evolves over the course of network training. The devices in this example all operate at the wavelength of 900 nm and deflection angle of 60 degrees, and 100 devices are randomly generated during each iteration of training. The high dimensional design space is visualized by performing a principle components analysis (PCA) on the binary metagratings dataset from adjoint-based optimization and then reducing the dimensionality of the space to two dimensions. The results are displayed in Figure 4 and Movie S1. Initially, the distribution of generated devices is spread broadly across the design space and the efficiency histogram spans a wide range of values, with most devices exhibiting low to modest efficiencies. As network training progresses, the distribution of generated devices more tightly clusters and

the efficiency histogram narrows at high efficiency values. By the 10,000 iteration mark, the generated devices have very high efficiencies and have converged to nearly the same device layout. A similar analysis for devices operating with other wavelength and angle combinations is presented in Figure S3.

An examination of total computation time indicates that GLOnet is computationally efficient at simultaneously optimizing a broad range of devices operating at different wavelengths and angles. The total number of simulations to train GLOnet is 1,200,000: the network trains over 30,000 iterations, uses batch sizes of $M = 20$ device instances per iteration, and uses a forward and adjoint simulation per device to compute its efficiency gradient. When divided by the 150 unique wavelength and angle combinations displayed in Figures 3a and 3b, the number of simulations per wavelength and angle pair is 8,000, which amounts to 20 adjoint-based topology optimization runs (one run has 200 iterations and 2 simulations/iteration). As a point of comparison, 500 adjoint-based topology optimization runs were required to produce each point in Figure 3a.

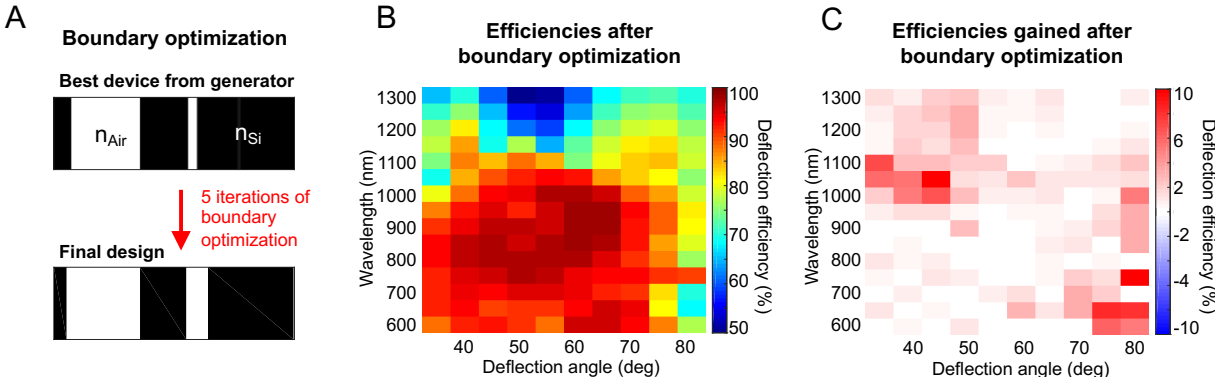


Figure 5: **Device refinement using boundary optimization.** (A) Boundary optimization uses efficiency gradients to refine the boundaries of binary structures. (B) Efficiency plot of devices generated by GLOnet and then refined with 5 iterations of boundary optimization. For this plot, the best device from Figure 3b for each wavelength and angle combination is used for boundary optimization. (C) Plot of gains in efficiency after boundary optimization, calculated from the data in Figure 3b and Figure 5b. Most devices experience modest boosts in efficiency, and 8% of devices exhibit over a 5% efficiency improvement.

Finally, we show that the generated devices from GLOnet can be further refined using

adjoint-based boundary optimization (Figure 5a). In this algorithm, the gradient of efficiency with respect to refractive index is calculated by conducting a forward and adjoint simulation, which is consistent with topology optimization. However, we only consider the gradients at the silicon-air boundaries of the device and fix the device refractive indices to be binary throughout the optimization. For this analysis, we perform 5 iterations of boundary optimization on the highest efficiency generated device for each wavelength and angle pair (Figure 3b). The final device efficiencies after boundary optimization are shown in Figure 5b and the differential changes in efficiency are shown in Figure 5c. Most of the efficiency changes are relatively modest and only 8% of devices have efficiency gains larger than 5%, indicating that devices from GLOnet are already at or near local optima.

Conclusions

In summary, we have shown that GLOnet is an effective and computationally-efficient global topology optimizer for metagratings. A global search through the design space is possible because the generative neural network optimizes the efficiencies of device distributions that initially span the design space. The best devices generated by GLOnet compare well with the best devices generated by adjoint-based topology optimization. Future work will focus on refining the mathematical theory behind this optimization method and improving parameters such as the network architecture, input noise characteristics, and training parameters, to make GLOnet higher performing and more robust to stochastic variations in training. Future work will also focus on extending GLOnet to other metasurface systems, including aperiodic, broadband devices. Given the generality of our approach, we envision that GLOnets can apply to the design of other classes of photonic devices and more broadly to other physical systems in which device performance can be improved using gradients.

Acknowledgement

The simulations were performed in the Sherlock computing cluster at Stanford University. This work was supported by the U.S. Air Force under Award Number FA9550-18-1-0070, the Office of Naval Research under Award Number N00014-16-1-2630, and the David and Lucile Packard Foundation. Competing interests: Authors declare no competing interests.

Supporting Information Available

The following files are available free of charge.

- Network architecture and training process of GLOnet
- Figures S1 to S3
- Tables S1
- Movie S1

References

- (1) Yu, N.; Capasso, F. Flat optics with designer metasurfaces. *Nature materials* **2014**, *13*, 139.
- (2) Kildishev, A. V.; Boltasseva, A.; Shalaev, V. M. Planar photonics with metasurfaces. *Science* **2013**, *339*, 1232009.
- (3) Kuznetsov, A. I.; Miroshnichenko, A. E.; Brongersma, M. L.; Kivshar, Y. S.; Luk'yanchuk, B. Optically resonant dielectric nanostructures. *Science* **2016**, *354*, aag2472.
- (4) Zheng, G.; Mühlenbernd, H.; Kenney, M.; Li, G.; Zentgraf, T.; Zhang, S. Metasurface holograms reaching 80% efficiency. *Nature nanotechnology* **2015**, *10*, 308.

- (5) Colburn, S.; Zhan, A.; Majumdar, A. Metasurface optics for full-color computational imaging. *Science advances* **2018**, *4*, eaar2114.
- (6) Arbabi, E.; Kamali, S. M.; Arbabi, A.; Faraon, A. Full-Stokes imaging polarimetry using dielectric metasurfaces. *ACS Photonics* **2018**, *5*, 3132–3140.
- (7) Tittl, A.; Leitis, A.; Liu, M.; Yesilkoy, F.; Choi, D.-Y.; Neshev, D. N.; Kivshar, Y. S.; Altug, H. Imaging-based molecular barcoding with pixelated dielectric metasurfaces. *Science* **2018**, *360*, 1105–1109.
- (8) Estakhri, N. M.; Edwards, B.; Engheta, N. Inverse-designed metastructures that solve equations. *Science* **2019**, *363*, 1333–1338.
- (9) others, et al. Highly tunable refractive index visible-light metasurface from block copolymer self-assembly. *Nature communications* **2016**, *7*, 12911.
- (10) Singh, R.; Cao, W.; Al-Naib, I.; Cong, L.; Withayachumnankul, W.; Zhang, W. Ultrasensitive terahertz sensing with high-Q Fano resonances in metasurfaces. *Applied Physics Letters* **2014**, *105*, 171101.
- (11) Sell, D.; Yang, J.; Doshay, S.; Zhang, K.; Fan, J. A. Visible light metasurfaces based on single-crystal silicon. *ACS Photonics* **2016**, *3*, 1919–1925.
- (12) Campbell, S. D.; Sell, D.; Jenkins, R. P.; Whiting, E. B.; Fan, J. A.; Werner, D. H. Review of numerical optimization techniques for meta-device design. *Optical Materials Express* **2019**, *9*, 1842–1863.
- (13) Rogers, E. T.; Lindberg, J.; Roy, T.; Savo, S.; Chad, J. E.; Dennis, M. R.; Zheludev, N. I. A super-oscillatory lens optical microscope for subwavelength imaging. *Nature materials* **2012**, *11*, 432.

- (14) Yin, J. Y.; Wan, X.; Zhang, Q.; Cui, T. J. Ultra wideband polarization-selective conversions of electromagnetic waves by metasurface under large-range incident angles. *Scientific reports* **2015**, *5*, 12476.
- (15) Jafar-Zanjani, S.; Inampudi, S.; Mosallaei, H. Adaptive genetic algorithm for optical metasurfaces design. *Scientific reports* **2018**, *8*, 11040.
- (16) Jensen, J. S.; Sigmund, O. Topology optimization for nano-photonics. *Laser & Photonics Reviews* **2011**, *5*, 308–321.
- (17) Molesky, S.; Lin, Z.; Piggott, A. Y.; Jin, W.; Vucković, J.; Rodriguez, A. W. Inverse design in nanophotonics. *Nature Photonics* **2018**, *12*, 659.
- (18) Sell, D.; Yang, J.; Wang, E. W.; Phan, T.; Doshay, S.; Fan, J. A. Ultra-high-efficiency anomalous refraction with dielectric metasurfaces. *ACS Photonics* **2018**, *5*, 2402–2407.
- (19) Yang, J.; Sell, D.; Fan, J. A. Freeform metagratings based on complex light scattering dynamics for extreme, high efficiency beam steering. *Annalen der Physik* **2018**, *530*, 1700302.
- (20) Lin, Z.; Groever, B.; Capasso, F.; Rodriguez, A. W.; Lončar, M. Topology-optimized multilayered metaoptics. *Physical Review Applied* **2018**, *9*, 044030.
- (21) Sell, D.; Yang, J.; Doshay, S.; Fan, J. A. Periodic Dielectric Metasurfaces with High-Efficiency, Multiwavelength Functionalities. *Advanced Optical Materials* **2017**, *5*, 1700645.
- (22) Xiao, T. P.; Cifci, O. S.; Bhargava, S.; Chen, H.; Gissibl, T.; Zhou, W.; Giessen, H.; Toussaint Jr, K. C.; Yablonovitch, E.; Braun, P. V. Diffractive spectral-splitting optical element designed by adjoint-based electromagnetic optimization and fabricated by femtosecond 3D direct laser writing. *ACS Photonics* **2016**, *3*, 886–894.

- (23) Piggott, A. Y.; Lu, J.; Lagoudakis, K. G.; Petykiewicz, J.; Babinec, T. M.; Vučković, J. Inverse design and demonstration of a compact and broadband on-chip wavelength demultiplexer. *Nature Photonics* **2015**, *9*, 374.
- (24) Hughes, T. W.; Minkov, M.; Williamson, I. A.; Fan, S. Adjoint method and inverse design for nonlinear nanophotonic devices. *ACS Photonics* **2018**, *5*, 4781–4787.
- (25) Lalau-Keraly, C. M.; Bhargava, S.; Miller, O. D.; Yablonovitch, E. Adjoint shape optimization applied to electromagnetic design. *Optics express* **2013**, *21*, 21693–21701.
- (26) Peurifoy, J.; Shen, Y.; Jing, L.; Yang, Y.; Cano-Renteria, F.; DeLacy, B. G.; Joannopoulos, J. D.; Tegmark, M.; Soljačić, M. Nanophotonic particle simulation and inverse design using artificial neural networks. *Science advances* **2018**, *4*, eaar4206.
- (27) Inampudi, S.; Mosallaei, H. Neural network based design of metagratings. *Applied Physics Letters* **2018**, *112*, 241102.
- (28) Ma, W.; Cheng, F.; Liu, Y. Deep-learning-enabled on-demand design of chiral metamaterials. *ACS nano* **2018**, *12*, 6326–6334.
- (29) Liu, D.; Tan, Y.; Khoram, E.; Yu, Z. Training deep neural networks for the inverse design of nanophotonic structures. *ACS Photonics* **2018**, *5*, 1365–1369.
- (30) Liu, Z.; Zhu, D.; Rodrigues, S. P.; Lee, K.-T.; Cai, W. Generative model for the inverse design of metasurfaces. *Nano letters* **2018**, *18*, 6570–6576.
- (31) Jiang, J.; Sell, D.; Hoyer, S.; Hickey, J.; Yang, J.; Fan, J. A. Data-driven metasurface discovery. *arXiv preprint arXiv:1811.12436* **2018**,
- (32) Yang, J.; Fan, J. A. Topology-optimized metasurfaces: impact of initial geometric layout. *Optics letters* **2017**, *42*, 3161–3164.
- (33) Hugonin, J.; Lalanne, P. RETICOLO CODE 2D. *Institute d’Optique, Palaiseau, France* **2005**,